

Large phonon band-gap in SrTiO₃ and the vibrational signatures of ferroelectricity in ATiO₃ perovskite: First principles lattice dynamics and inelastic neutron scattering of PbTiO₃, BaTiO₃ and SrTiO₃.

Narayani Choudhury¹, Eric J. Walter², Alexander I. Kolesnikov³ and Chun-Keung Loong³

¹*Solid State Physics Division, Bhabha Atomic Research Centre, Trombay, Mumbai 400085, India*

²*College of William and Mary, Williamsburg, Virginia 23187, USA*

³*Intense Pulsed Neutron Source Division, Argonne National Laboratory, Argonne, Illinois 60439, USA*

Abstract

We report first principles density functional perturbation theory calculations and inelastic neutron scattering measurements of the phonon density of states, dispersion relations and electromechanical response of PbTiO₃, BaTiO₃ and SrTiO₃. The phonon density-of-states of the quantum paraelectric SrTiO₃ is found to be fundamentally distinct from that of ferroelectric PbTiO₃ and BaTiO₃ with a large 70-90 meV phonon band-gap. The phonon dispersion and electromechanical response of PbTiO₃ reveal giant anisotropies. The interplay of covalent bonding and ferroelectricity, strongly modulates the electromechanical response and give rise to spectacular signatures in the phonon spectra. The computed charge densities have been used to study the bonding in these perovskites. Distinct bonding characteristics in the ferroelectric and paraelectric phases give rise to spectacular vibrational signatures. While a large phonon band-gap in ATiO₃ perovskites seems a characteristic of quantum paraelectrics, anisotropy of the phonon spectra correlates well with ferroelectric strength. These correlations between the phonon spectra and ferroelectricity, can guide future efforts at custom designing still more effective piezoelectrics for applications. These results suggest that vibrational spectroscopy can help design novel materials.

I. Introduction

Ferroelectric materials interconvert electrical and mechanical energies and find key technological applications¹ as piezoelectric transducers and actuators used in ultrasonic devices, medical imaging and telecommunications. Classic perovskites like PbTiO₃, BaTiO₃ and SrTiO₃ present unusual properties and puzzles¹⁻²³ and their first principles calculations²⁻¹² and experiments¹³⁻²³ have helped elucidate a wide range of fundamental issues like the electronic origins of ferroelectricity³, soft phonon modes and structural phase transitions^{1,13}, giant LO-TO (longitudinal optic-transverse optic) splittings⁷ and vibrational anomalies⁴⁻⁹, origin of ultrahigh electromechanical response¹⁰, *etc.* SrTiO₃ is an incipient ferroelectric with a very large static dielectric response, which exhibits remarkable phonon anomalies^{5,18} and electrostrictive response¹⁹. The ferroelectric phase in SrTiO₃ is suppressed even as $T \rightarrow 0$ K by zero-point fluctuations leading to quantum paraelectricity¹⁵.

Both PbTiO₃ and BaTiO₃ have a simple cubic high temperature paraelectric phase which transforms to a ferroelectric tetragonal phase around 763 K and 403 K, respectively¹. Tetragonal PbTiO₃ is a large strain material ($c/a=1.06$) which is ferroelectric even at high temperatures, and exhibits a single cubic to tetragonal transition. BaTiO₃ on the other hand has a much smaller strain (1.01) and exhibits successive phase transitions from cubic to tetragonal, orthorhombic and rhombohedral structures with decreasing temperature. SrTiO₃ undergoes a transition from the cubic ($Pm\bar{3}m$) to a tetragonal ($I4/mcm$) antiferrodistortive phase at 105 K; however this transition has a non-polar character and does not affect its dielectric properties. Electronic structure calculations³ reveal that intrinsic differences in the bonding in tetragonal BaTiO₃ and PbTiO₃, give rise to their vastly different phase diagram and ferroelectric behavior.

In this work, we report *ab initio* lattice dynamics calculations and inelastic neutron scattering studies of the complete phonon dispersion relations, density of states and electromechanical response of three classic perovskites: ferroelectric PbTiO₃ and BaTiO₃ and the quantum paraelectric SrTiO₃. The experimental and theoretical determination of the phonon density of states and dispersion relations gives access to valuable quantitative information concerning elasticity, piezoelectric and dielectric behavior, thermodynamic properties and the dynamics of soft-mode driven phase instabilities. The fundamental interest, distinct ferroelectric behavior and important applications make PbTiO₃, BaTiO₃ and SrTiO₃ highly suitable for these studies. Our goals are, (i) to understand the vibrational signatures of ferroelectricity, (ii) to study the interplay between the structure, bonding, dynamics and electromechanical response, and, (iii) to identify the factors that govern enhanced piezoelectric response, required for the design of new materials. The neutron measurements provide a critical test for the theory. The integration of first principles calculations and vibrational spectroscopic experiments provide important insights on the correlations between vibrational spectra and ferroelectricity, and illustrate how vibrational spectroscopic techniques can lead to the design of novel materials.

Several workers²⁰ have reported inelastic neutron scattering measurements of the phonon dispersion relations and have studied the temperature variations of the soft phonon mode across the ferroelectric to paraelectric transition in these perovskites. The phonon dispersion relations data are however incomplete especially in the lower symmetry ferroelectric phases. Even in the high symmetry paraelectric cubic phase, the dispersion relations of only the acoustic and low frequency optic phonon branches have been measured²⁰. Thus far, first principles calculations of the complete phonon dispersion relations are reported only for the cubic phases^{2,6} of PbTiO₃, BaTiO₃ and SrTiO₃. A thorough understanding of the phonon dispersion relations in the ferroelectric phases is essential for a microscopic understanding of their electromechanical properties and for resolving the controversies about the origin of diffuse scattering²³ in perovskite ferroelectrics and have formed the focus of this work. In spite of a flurry of reported research on these perovskites¹⁻²³, studies of the complete phonon density of states and systematic examinations of the vibrational signatures of ferroelectricity, *etc.* were not earlier studied. Systematic examination of these various issues which form the fundamental link between the microscopic physics and macroscopic material behavior is the key to defining new experimental

protocols for the screening and design of novel functional materials. Classic perovskites like PbTiO_3 , BaTiO_3 and SrTiO_3 which have served as a fertile ground for the discovery of new physical phenomena and devices¹⁻²³ are ideal model systems for such studies.

II. Techniques

A. Theoretical studies

We have undertaken first principles calculations of ferroelectric tetragonal PbTiO_3 and rhombohedral BaTiO_3 with space groups $P4mm$ and $R3m$ and the paraelectric cubic ($Pm\bar{3}m$) and antiferrodistortive tetragonal phases ($I4/mcm$) of SrTiO_3 (ST). Density functional theory (DFT) permits calculation of the total energy of solids without any parameterization to experimental data. The phonon spectra, elastic, piezoelectric and dielectric tensors are related to the second derivatives of the total energy with respect to variables like atomic displacements, macroscopic strain, and electric field. All these material properties can be efficiently computed using density functional perturbation theory (DFPT)²⁴⁻²⁷. The dielectric susceptibility and elastic constants involve second derivatives of total energy with respect to electric field and strain, respectively, while the piezoelectric tensor is the mixed second derivative of total energy with respect to strain and electric field. DFPT linear response studies have intrinsic advantages over the frozen phonon technique, as they do not require large supercells for the studies of phonons at a general wavevector. Furthermore, the DFPT approach includes explicit treatment of the long ranged Coulomb interactions, required to obtain accurate values of the LO-TO splittings.

We carried out DFT and DFPT linear response calculations using plane wave basis sets and the code ABINIT²⁸ using the local density approximation (LDA). These calculations used norm-conserving pseudopotentials²⁹⁻³² generated using the code OPIUM. The pseudopotential results were rigorously tested³¹ against the full-potential linearized augmented plane-wave calculations and included semicore states of Pb $5d^{10}$, Ti $3s^23p^64d^2$, and O $2s^2$ as valence states. The Brillouin zone integrations were performed with a $6 \times 6 \times 6$ \mathbf{k} -point mesh using a plane-wave energy cut off of 120 Rydbergs. We first carried out full structural relaxations for these perovskites. Linear response DFPT studies²⁴⁻²⁶ using a $6 \times 6 \times 6$ \mathbf{k} -point grid with atomic displacements, strain and electric field perturbations were used to compute the zone center phonon frequencies, elastic, piezoelectric and dielectric properties. The spontaneous polarization was computed using the Berry's phase approach²⁷ using a $6 \times 6 \times 20$ \mathbf{k} -point grid, with a dense mesh along the direction of polarization. All calculations are at zero temperature.

To study the phonons at a general wavevector, response functions were calculated on a $4 \times 4 \times 4$ grid of \mathbf{q} -points in the Brillouin zone (BZ), including the zone center Γ point. The phonon frequencies at a general wavevector \mathbf{q} were obtained by interpolating the dynamical matrices calculated on this grid. The phonon density of states involves an integrated average over the phonon modes in the entire Brillouin zone and is given by,

$$g(\omega) = A \int_{BZ} \sum_j \delta(\omega - \omega_j(\mathbf{q})) d\mathbf{q}$$

where A is a normalization constant such that $\int g(\omega) d\omega = 1$ and $\omega_j(\mathbf{q})$ is the frequency of the j^{th} phonon mode. We used a $12 \times 12 \times 12$ \mathbf{q} -point mesh in the irreducible Brillouin zone to calculate the phonon density of states.

B. Experimental studies

We have carried out inelastic neutron scattering measurements ($T=6$ K) of the phonon density of states of three classic perovskites: ferroelectric PbTiO_3 and BaTiO_3 and the quantum paraelectric SrTiO_3 . The inelastic neutron scattering measurements were carried out using powder samples on the High-Resolution Medium-Energy Chopper Spectrometer (HRMECS) using the time-of-flight technique at Argonne's Intense Pulsed Neutron Source. Two incident neutron energies were used (50 and 130 meV) to obtain good resolution data in all range of energy transfers. The data were collected over a wide range of scattering angles (28° to 132°) for large coverage of momentum transfers. The high energies of neutrons from pulsed sources enable measurements of the phonon spectra over its entire energy range. Samples were cooled to 6 K using a conventional liquid-helium cryostat with the sample to minimize multiphonon contributions. The energy resolution ΔE (full width at half maximum) of the HRMECS spectrometer varies between 2–6% of the incident-neutron energy (E_0) over the neutron-energy-loss region. The data were corrected for background scattering by subtracting the results from empty container runs. Measurements of the elastic incoherent scattering from a vanadium standard provided the detector calibration and intensity renormalization.

The observed data were analyzed in the incoherent approximation^{33,34}, wherein the measured scattering function $S(Q, E)$ in the neutron energy loss experiments is related to the generalized density of states by³⁴

$$g^n(E) = B \left\langle \frac{e^{2W(Q)}}{Q^2} \frac{E}{n(E, T) + 1} S(Q, E) \right\rangle \approx C \sum_k \left\{ \frac{4\pi b_k^2}{m_k} \right\} g_k(E)$$

where the partial density of states $g_k(E)$ is given by $g_k(E) = D \int_{BZ} \sum_j |\xi(\mathbf{q}, k)|^2 \delta(E - E_j(\mathbf{q})) d\mathbf{q}$ and $n(E, T) = [\exp(E/k_B T) - 1]^{-1}$. B, C and

D are normalization constants. b_k and m_k are respectively, the neutron scattering-length and mass of the k^{th} atom. $E_j(\mathbf{q})$ and $\xi(\mathbf{q}, j)$ respectively correspond to the energy and eigenvector of the j^{th} phonon mode at wavevector \mathbf{q} in the BZ. The symbol $\langle \rangle$ represents Q averaging of the quantities within.

The incoherent approximation^{33, 34} is valid, when the ratio of the volume of the reciprocal space covered in the experiment to the volume of the Brillouin zone is large. In our inelastic neutron scattering experiment, this ratio was about a few thousands. The data were properly averaged over the range of scattering angles to obtain the neutron-weighted generalized phonon density of states $g^n(E)$. The first principles calculations were used to derive the generalized phonon density of states $g^n(E)$ for comparison with the experiments. The computed density of states were smeared with Gaussians having full width at half maximum of 1 meV for comparison with the experiments, due to the finite resolution involved in the measurements.

III. Results

A. Phonon dispersion relations and long wavelength phonon frequencies

The calculated phonon dispersion relations of PbTiO₃ (Fig. 1) reveal giant anisotropies and span distinct spectral ranges for wavevector directions along (Γ -Z-A-R-Z) and perpendicular (Γ -M-X- Γ) to the direction of spontaneous polarization. Very limited single crystal inelastic neutron data²⁰ and first principles calculations⁴ of the phonon frequencies of PbTiO₃ were earlier reported and are in good agreement with our studies (Table I). The calculated transverse acoustic and transverse optic modes of PbTiO₃ (Fig. 1) propagating in the direction perpendicular to the spontaneous polarization show considerable splitting due to tetragonal anisotropy in agreement with reported inelastic neutron data^{20(b)}. LDA calculations of PbTiO₃ underestimate the strain (calculated $c/a=1.047$, observed $c/a=1.063$) and volume (calculated $V=60.4 \text{ \AA}^3$). As the phonon frequencies are quite sensitive to the structural parameters, we have relaxed the structural variables of PbTiO₃ at the observed lattice constants, as in earlier studies⁴. The computed structural parameters and long wavelength phonon frequencies of tetragonal PbTiO₃ and rhombohedral BaTiO₃ are found to be in good agreement with reported experimental data^{17(c),22(a)} and LDA calculations^{4,26(b)} (Table I). The phonon dispersion relations of rhombohedral BaTiO₃ are plotted along cubic high symmetry directions (Fig. 1), to enable direct comparisons with the $\omega_j(\mathbf{q})$ of tetragonal PbTiO₃.

Symmetry analysis of the zone-center Γ -point phonon modes for the $P4mm$ space group of PbTiO₃ yields the classification $\Gamma: 4A_1+5E+B_1$. The E symmetry phonon modes are doubly degenerate. The A₁ and E phonon modes which are both Raman and infrared active, are polar modes with vibrations which are respectively parallel and perpendicular to the direction of spontaneous polarization. For rhombohedral BaTiO₃, the phonon modes can be classified as $\Gamma: 4A_1+5E+A_2$. The A₁ and 4 E modes are polar while the A₂ mode and a doubly degenerate E-mode are non-polar (Table I). While most of the calculated frequencies of PbTiO₃ are in good agreement with experiments (Table I), the observed E-symmetry polar infrared-active phonon modes^{22(a)} at 289 (TO), 505 (TO) and 723 (LO) cm⁻¹ at the Γ point are underestimated, which causes the shifting of the corresponding branches/peaks in the computed phonon dispersion relations and phonon density of states of PbTiO₃ (Figs. 1, 2). Nevertheless, LDA calculations of PbTiO₃ bring out all the salient features and the calculated phonon dispersion relations and density of states are overall in good agreement with experiments.

Although experimentally SrTiO₃ is not ferroelectric even at low temperatures, it is very close to the ferroelectric threshold. Isotopic replacement of oxygen or partial cation substitution reduces quantum fluctuations and makes it ferroelectric¹⁴. Path-integral Monte-Carlo simulations which include zero-point energy contributions yield the correct ground state⁸ for ST. Neglect of zero-point energy in the structural relaxation, yields ferroelectric zone center instabilities for the polar E_u and A_{2u} phonon modes in the tetragonal $I4/mcm$ antiferrodistortive structure in agreement with earlier reports⁵. LDA calculations of cubic SrTiO₃ yields soft zone center and zone boundary R and M point phonon instabilities in good agreement with reported all electron linear augmented plane wave calculations⁶. LDA calculations on a coarse wavevector mesh of the antiferrodistortive phase suggest that the phonon density of states of the tetragonal antiferrodistortive and cubic phases are overall quite similar.

Stirling *et al.*^{20(g)} and Cowley²⁰⁽ⁱ⁾ have reported single crystal inelastic neutron scattering measurements at T=90 K and T=296 K of the low energy crystal dynamics and phonon dispersion relations in SrTiO₃. They have fitted the observed inelastic neutron data to several lattice dynamics models with temperature dependent force constants^{20(g), 20(i)}. SrTiO₃ exhibits dynamical critical phenomena in the vicinity of the low temperature phase transition and the temperature variations of the soft mode phonon frequencies and lineshapes have aroused considerable interest^{20(j)}. Our computed *ab initio* T=0 K phonon dispersion relations of cubic SrTiO₃ are compared with the reported T=90 K inelastic neutron scattering data^{20(g), 20(i)} (Fig. 1(c)). Our calculations of cubic SrTiO₃ reveal very strong dispersion of the lowest energy optic phonon modes along ($\xi\xi\xi$) and ($\xi\xi 0$) wavevector directions, in good agreement with reported inelastic neutron experiments^{20(g), 20(i)} (Fig. 1(c)). While the higher frequency optic modes are in satisfactory agreement, the observed zone center, R and M point soft modes in SrTiO₃ [which are found to be strongly temperature dependent^{20(g), 20(i)}] are in qualitative agreement with our T=0 K calculations. The computed phonon density of states of cubic and tetragonal SrTiO₃ neglecting effects from phonon instabilities are found to be in good agreement with our measured inelastic neutron scattering T=6 K data (Fig. 2).

B. Calculated charge densities and bonding characteristic of PbTiO₃, BaTiO₃ and SrTiO₃

The computed charge densities and isosurface plots of tetragonal PbTiO₃ and rhombohedral BaTiO₃ are given in Fig. 3. All densities were computed from the fully relaxed zero pressure LDA structures. The well connected region of charge between the Pb and O atoms indicate the strong covalent Pb-O bonding in PT. In BaTiO₃, the charge densities almost connect (Fig. 3) while in

cubic SrTiO₃ they are far from connecting which reveal ionic Ba-O and Sr-O bonding, respectively. Electronic structure calculations³ reveal that the covalent bonding between the Ti and O in PbTiO₃ and BaTiO₃ arise from the hybridization between the titanium 3*d* states and the oxygen 2*p* states. This covalent Ti-O bonding was found to be essential for ferroelectricity in perovskites³. The strong covalency of the Pb-O bonds in tetragonal PbTiO₃ which arises from the hybridization of the Pb 6*s* state and O 2*p* state has been theoretically predicted³ as a key factor of the much larger ferroelectricity of PbTiO₃ as compared to BaTiO₃. The covalent character of the Pb-O bonds have been experimentally verified¹⁶ and the computed charge densities are in good agreement with the observed density distributions of tetragonal PbTiO₃ and BaTiO₃ obtained from maximum entropy analysis of synchrotron data. The covalent nature of the Pb-O bond stabilizes the ferroelectric tetragonal phase in PbTiO₃, while the ionic nature of the Ba-O bond stabilizes the rhombohedral phase of BaTiO₃. These structural and bonding changes in these materials lead to important differences in their PDR (Fig. 1), PDOS (Fig. 2) as well as elastic, piezoelectric and dielectric properties (Table II).

C. Elastic, piezoelectric and dielectric properties

The computed elastic, piezoelectric and dielectric properties of PbTiO₃ at the experimental volume (Table II) are in good agreement with reported room temperature Brillouin scattering data³⁵. These demonstrate the intrinsic ability of DFPT calculations in accounting for acoustic phonons and polarization accurately. Electronic structure calculations³ reveal that the hybridization between the titanium 3*d* states and the oxygen 2*p* states is essential for ferroelectricity in perovskites. The strong covalent character of the Pb-O bond (Fig. 3) in PbTiO₃ enhances its ferroelectric strength³ as compared to BaTiO₃, wherein the Ba-O bonding is ionic. These bonding changes³ between PbTiO₃ and BaTiO₃ give rise to significant differences in their Curie temperature, phase diagram and electromechanical response (Table II). The large difference between the elastic constants C_{33} and C_{11} (Table II) in tetragonal PbTiO₃ reflects its inherent large anisotropy. This anisotropy is due to the large difference in the longitudinal acoustic phonon wave velocities, for propagation along and perpendicular to the direction of polarization (Fig. 1). This anisotropy in PbTiO₃ leads to interesting directional enhancements of its piezoresponse (Table II). The enhanced values for e_{33} and e_{15} in tetragonal PbTiO₃ are due to the large atomic response to the corresponding macroscopic strains combined with large anomalous values of the Born effective charge tensors.

The computed partial density of states giving the dynamical contributions from various atoms are given in Fig. 4. These reveal that the 0-20 meV low frequency vibrations which critically govern the electromechanical response are strongly influenced by the A-O bonding character. The strong covalent bonding of the Pb-O bonds (Fig. 3) contributes to the strong anisotropy of the elastic and piezoelectric response of PbTiO₃ (Table II). Although first principles calculations of the piezoelectric response in PbTiO₃ and BaTiO₃ have also been reported by others^{11,26}, in this work we have examined the intimate connections between phonon spectra and electromechanical response. The computed elastic, piezoelectric and dielectric constants (Tables I, II) are found to be quite sensitive to the relaxed structural parameters and although our results for PbTiO₃ are similar to earlier first principles results¹¹, our results for BaTiO₃ have some differences with reported values^{26(b)} which are due to the differences in their computed crystal structures.

D. Phonon density of states and partial density of states

The computed generalized phonon density of states is in good agreement with the observed inelastic neutron scattering spectra (Fig. 2) and spans the spectral range from 0-120 meV. The phonon spectrum of the quantum paraelectric SrTiO₃ is found to be fundamentally distinct from those of ferroelectric PbTiO₃ and BaTiO₃, with a large 70-90 meV phonon band-gap. This large phonon band-gap is due to the distinct bonding in SrTiO₃ (Fig. 3) as compared to ferroelectric PbTiO₃ and BaTiO₃. From the viewpoint of crystal stability^{9, 14}, the quantum paraelectricity in the threshold of ferroelectric behavior in SrTiO₃ originates from the critical status of this material. Such trends are conventionally studied^{9, 14} using the tolerance factor ($t = (r_{Sr} + r_O) / \sqrt{2} (r_{Ti} + r_O)$). Using reported ionic radii, the tolerance was found to be $t = 1.00$ for SrTiO₃, which means that the ion packing in SrTiO₃ is ideal for a perovskite-type structure¹⁴. The tolerance t for BaTiO₃ and PbTiO₃ are similarly⁹, 1.07 and 1.03. Larger ($t > 1$) and smaller ($t < 1$) values were found to favor ferroelectricity [e.g. BaTiO₃] and quantum paraelectricity [eg, see Ref. [9]: CaTiO₃, $t = 0.97$], respectively. The critical status of SrTiO₃ and its distinct bonding as compared to PbTiO₃ and BaTiO₃, result in spectacular signatures in the phonon spectra.

The computed partial density of states (Fig. 4) enables microscopic interpretations of the observed data. These reveal that while the A-cations (namely, the Pb, Ba and Sr) contribute in the 0-20 meV spectral range (Fig. 4), the intermediate and high energy spectra are due to the Ti and O vibrations. The phonon spectra (neglecting instabilities) are overall similar in the paraelectric cubic and tetragonal antiferrodistortive phase of SrTiO₃ as the distortions for the SrO₁₂ and TiO₆ polyhedra are small in the antiferrodistortive tetragonal phase of SrTiO₃. On the other hand, the covalent Ti-O bonding, found essential for ferroelectricity in perovskites, causes a strong distortion of the Ti-O₆ octahedra and the spectra are significantly different in the ferroelectric and paraelectric phases of PbTiO₃ and BaTiO₃. For example, in tetragonal PbTiO₃, the calculated Ti-O bond lengths (Å) are 1.9785 (4), 1.7606 (1), 2.3908 (1), [where the values in parentheses give the multiplicity of the bonds] which deviate significantly from the typical Ti-O bond length of about 1.95 Å in cubic perovskites. This strong TiO₆ octahedral distortion (Table I) characteristic of ferroelectric behavior is responsible for the filling up of the characteristic 70-90 meV phonon band-gap of the quantum paraelectric SrTiO₃. Strong covalency of the Pb-O bonds, similarly distorts the PbO₈ polyhedra (2.8016(4) Å; 2.5243 (4) Å) in tetragonal PbTiO₃, which lead to the following: (i) The vibrations of the Pb atoms in PbTiO₃ (around 7.5 meV) are considerably softer than in the vibrations of Ba (around 12.5 meV) in BaTiO₃ and Sr (around 13 meV) in SrTiO₃, (ii) there are significant differences in the elastic and piezoelectric properties of PbTiO₃ and BaTiO₃ (Table II).

IV. Discussion

A large 70-90 meV phonon band-gap seems characteristic of ATiO₃ perovskite quantum paraelectrics like SrTiO₃. In the case of the ferroelectric instability, the covalent interactions which play a predominant role³ lead to marked differences in the phonon spectra. Ferroelectricity in perovskites arises from a competition between the Coulomb (which favors ferroelectric) and short-ranged (which favors paraelectric) interactions³. This competition which contributes to several reported anomalies^{2,23}, also leads to the spectacular signatures in the phonon spectra. The covalent Ti-O bonding (Fig. 3) found necessary for ferroelectric behavior in perovskites³ causes the following: (i) the large 70-90 meV phonon band-gap of paraelectric SrTiO₃ gets filled by the covalent Ti-O vibrations in ferroelectric PbTiO₃ and BaTiO₃, and (ii) there are giant anisotropies in the phonon spectra and electromechanical response of PbTiO₃ (due to the combined Ti-O and Pb-O covalent bonding). The anisotropy of the phonon spectra correlates well with ferroelectric and piezoelectric strength. These results suggest that vibrational spectroscopy can aid in the search for novel materials. The distinct phonon spectra of PbTiO₃, BaTiO₃ and SrTiO₃ lead to important differences in their thermodynamic properties and phase diagram.

An important objective of this study was the integration of current advances in first principles computational theory with neutron experiments to provide microscopic insights that can define new strategies for the screening of novel materials. To transform the theoretical quantum mechanical techniques²⁴⁻²⁷ developed in the last several decades into predictive design and discovery tools, important tests of the ability of modern first principles theory in reproducing various macroscopic physical properties of ferroelectrics were of interest. In this context, we have compared our calculations, with reported¹⁵⁻²³ Raman and infrared data (Table I), inelastic neutron data²⁰ (Figs. 1, 2), Brillouin data³⁵ (Table II) and synchrotron x-ray data¹⁶ of three classic perovskites in addition to comparing with our experimental neutron data. Our calculations are in good agreement with these experimental studies. The theoretical studies predict giant anisotropies in the phonon dispersion relations and electromechanical response of PbTiO₃ which arise due to the strongly “directional” character of the covalent interactions found necessary for ferroelectricity. This anisotropy in the phonon dispersion relations obtained from first principles calculations of PbTiO₃ (particularly for the high energy modes which have not been earlier studied [20]) is measurable experimentally via future single crystal inelastic neutron scattering and inelastic x-ray scattering measurements. Anisotropy in the phonon spectra of PbTiO₃ obtained from LO-TO (longitudinal optical- transverse optical) splittings have been measured using single-crystal infrared spectroscopic studies and are found to be in good agreement with our calculations (Table I).

V. Conclusions

In summary, we report very successful tests of the ability of first principles theory in reproducing the experimental data of phonon dispersion relations, density of states and electromechanical response of three classic perovskites PbTiO₃, BaTiO₃ and SrTiO₃. We obtain an important correlation between the phonon spectra and ferroelectricity in perovskites, which can guide future efforts at custom designing still more effective piezoelectrics for applications. A large phonon band-gap seems characteristic of ATiO₃ perovskite quantum paraelectrics, while anisotropy of the phonon spectra correlates well with ferroelectric strength. Distinct bonding characteristics in the ferroelectric and paraelectric phases give rise to these vibrational signatures. Although, we have studied only three classic perovskites, since the vibrational signatures we obtain arise due to fundamental differences in the physics of ferroelectrics (covalently bonded) and paraelectric systems, we believe that these correlations in phonon spectra could be universal. Our results suggest that vibrational spectroscopy can aid in the search for novel materials. We hope these studies will stimulate interest in systematic investigations of other ferroelectrics to examine the universalities of our observations. The excellent agreement between theory and experiments, demonstrate the intrinsic power of first principles quantum mechanical calculations for deriving various key properties of these materials.

Acknowledgements

N.C. thanks R. E. Cohen and S.L. Chaplot for discussions. This research used the supercomputing resources at the Bhabha Atomic Research Centre (BARC) and the Center for Piezoelectrics by Design, College of William and Mary (E.J.W.). The work at Argonne National Laboratory was supported by the Office of Basic Energy Sciences, Division of Materials Sciences, U.S. Department of Energy, under Contract No. W-31-109-ENG-38.

References

- ^{1(a)}M.E. Lines and A.M. Glass, *Principles and Applications of Ferroelectrics and related materials*, (Clarendon, Oxford) (1977);
- ^(b)F. Jona and G. Shirane, *Ferroelectric Crystals*, Dover, New York, 1993.
- ²P. Ghosez, E. Cockayne, U. V. Waghmare, and K. M. Rabe, *Phys. Rev. B* **60**, 836 (1999).
- ³R.E. Cohen, *Nature* (London) **358**, 136 (1992).
- ⁴A. García and D. Vanderbilt, *Phys Rev B* **54**, 3817 (1996).
- ⁵N. Sai and D.Vanderbilt, *Phys. Rev. B* **62**, 13942 (2000).
- ⁶C. Lasota, C. -Z. Wang, R. Yu, and H. Krakauer, *Ferroelectrics* **194**, 109 (1997).
- ⁷W. Zhong, R.D. King-Smith, and D.Vanderbilt, *Phys. Rev. Lett.* **72**, 3618 (1994).
- ⁸W. Zhong and D. Vanderbilt, *Phys. Rev. B* **53**, 5047 (1996).
- ⁹W. Zhong and D. Vanderbilt, *Phys. Rev. Lett.* **74**, 2587 (1995).
- ¹⁰H. Fu and R.E. Cohen, *Nature* (London) **403**, 281 (2000).
- ¹¹Z. Wu and R.E. Cohen, *Phys. Rev. Lett.* **95**, 037601 (2005); G. Sághi-Szabó, R.E. Cohen and H. Krakauer, *Phys. Rev. Lett.* **80**, 4321 (1998).
- ¹²I. A. Kornev, L. Bellaiche, P. Bouvier, P.-E. Janolin, B. Dkhil, and J. Kreisel, *Phys. Rev. Lett.* **95**, 196804 (2005); I. I. Naumov

- and H. Fu, Phys. Rev. B **72**, 012304 (2005); H. Fu and L. Bellaïche, Phys. Rev. Lett. **91**, 057601 (2003); B.P. Burton and E. Cockayne, Phys. Rev. B **60**, R12542 (1999); M. Ghita, M. Fornari, D. J. Singh, and S. V. Halilov, Phys. Rev. B **72**, 054114 (2005).
- ¹³M. Ahart, M. Somayazulu, R. E. Cohen, P. Ganesh, P. Dera, H.K. Mao, R. J. Hemley, Y. Ren, P. Liermann and Z. Wu, Nature **451**, 543 (2008).
- ¹⁴M. Itoh, R. Wang, Y. Inaguma, T. Yamaguchi, Y-J. Shan, and T. Nakamura, Phys. Rev. Lett. **82**, 3540 (1999).
- ¹⁵K.A. Muller and H. Burkard, Phys. Rev. B **19**, 3593 (1979)
- ¹⁶Y. Kuroiwa, S. Aoyagi, A. Sawada, J. Harada, E. Nishibori, M. Takata, and M. Sakata, Phys. Rev. Lett. **87**, 217601 (2001).
- ¹⁷(^a) B.Zalar, V.V. Laguta and R. Blinc, Phys. Rev. Lett. **90**, 037601 (2003); (^b) E.A. Stern, Phys. Rev. Lett. **93**, 037601(2004); (^c) M. Dawber, C. Lichtensteiger, M. Cantoni, M. Veithen, P. Ghosez, K. Johnston, K. M. Rabe, and J.-M. Triscone, Phys. Rev. Lett. **95**, 177601 (2005).
- ¹⁸A. A. Sirenko, I. A. Akimov, J. R. Fox, A. M. Clark, H. C. Li, W. Si, and X. X. Xi, Phys. Rev. Lett. **82**, 4500 (1999).
- ¹⁹D.E. Grupp and A. M. Goldman, Phys. Rev. Lett. **78**, 3511 (1997).
- ²⁰(^a) I. Tomeno, Y. Ishii, Y.Tsunoda and K. Oka, Phys. Rev. B **73**, 064116 (2006); (^b)J. Hlinka, M. Kempa, J. Kulda, P. Bourges, A. Kania, and J. Petzelt, Phys. Rev. B **73**, 140101(R) (2006); (^c)G. Shirane, Rev. Mod. Phys. **46**, 437 (1974); (^d)G. Shirane, B. C. Frazer, V. J. Minkiewicz, and J. A. Leake, Phys. Rev. Lett. **19**, 234 (1967); (^e)G. Shirane, J. D. Axe, J. Harada, and J. P. Remeika, Phys. Rev. B **2**, 155 (1970); (^f)G. Shirane, J. D. Axe, J. Harada and A.Linz, Phys. Rev. B **2**, 3651 (1970); (^g)W.G. Stirling, J. Phys. C **5**, 2711 (1972); (^h)B Jannot, C Escribe-Filippini and J Bouillot, J. Phys. C**17**, 1329 (1984); (ⁱ) R.A. Cowley, Phys. Rev. **134**, A981 (1964); (^j) D.A. Bruce and W.G. Stirling, J. Phys. C **16**, 841 (1983).
- ²¹(^a)R.J. Nelmes and W.F. Kuhs, Solid State Communications **54**, 721 (1985); (^b)G. H. Kwei, A. C. Lawson, S. J. L. Billinge, and S.-W. Cheong, J. Phys. Chem.,**97**, 2368(1993);(^c)A. W. Hewat, Ferroelectrics **6**, 215 (1974); (^d)A. Sani, M. Hanfland and D. Levy, J. Phys.: Condens. Matter **14**, 10601(2002).
- ²²(^a) J. D. Freire and R. S. Katiyar, Phys. Rev. B **37**, 2074 (1988); (^b)C.M. Forster, M. Grimsditch, Z.Li, V.G. Karpov, Phys. Rev. Lett. **71**, 1258 (1993); (^c)J. Petzelt, T. Ostapchuk, I. Gregora, I. Rychetský, S. Hoffmann-Eifert, A. V. Pronin, Y. Yuzyuk, B. P. Gorshunov, S. Kamba, V. Bovtun, J. Pokorný, M. Savinov, V. Porokhonsky, D. Rafaja, P. Vaněk, A. Almeida, M. R. Chaves, A. A. Volkov, M. Dressel, and R. Waser, Phys. Rev. B **64**, 184111 (2001).
- ²³B. D. Chapman, E. A. Stern, S.-W. Han, J. O. Cross, G. T. Seidler, V. Gavril'yatchenko, R. V. Vedrinskii, and V. L. Kraizman, Phys. Rev. B **71**, 020102(R) (2005).
- ²⁴For a review on DFPT, see S. Baroni, S. de Gironcoli, A.D. Corso and P. Giannozzi, Rev. Mod. Phys. **73**, 515 (2001).
- ²⁵X. Gonze, Phys. Rev. B **55**, 10337 (1997); X. Gonze and C. Lee, Phys. Rev. B **55**, 10355 (1997).
- ²⁶(^a)D.R. Hamann, X. Wu, K. M. Rabe, and D. Vanderbilt, Phys. Rev. B **71**, 035117 (2005); (^b)X. Wu, D. Vanderbilt, and D. R. Hamann, Phys. Rev. **B72**, 035105 (2005); (^c)M. Veithen, X. Gonze, and Ph. Ghosez, Phys. Rev. B **71**, 125107 (2005).
- ²⁷R. Resta, Rev. Mod. Phys. **66**, 899 (1994); R.D. King-Smith and D. Vanderbilt, Phys. Rev. B **47**, 1651 (1993).
- ²⁸X. Gonze, J.-M. Beuken, R. Caracas, F. Detraux, M. Fuchs, G.-M. Rignanese, L. Sindic, M. Verstraete, G. Zerah, F. Jollet, M. Torrent, A. Roy, M. Mikami, Ph. Ghosez, J.-Y. Raty, D.C. Allan, Computational Materials Science **25**, 478 (2002); The ABINIT code is a collaborative project of the Universite Catholique de Louvain, Corning Inc. and other collaborators (URL: <http://www.abinit.org/>).
- ²⁹<http://www.sourceforge.net/>.
- ³⁰A.M. Rappe, K.M. Rabe, E. Kaxiras and J.D. Joannopoulos, Phys. Rev. B **41**, 1227 (1990).
- ³¹N. Choudhury, Z. Wu, E.J. Walter and R.E. Cohen, Phys. Rev. B **71**, 125134 (2005); N. Choudhury, R. E. Cohen, and E.J. Walter, Computational Materials Science **37**, 152 (2006).
- ³²N. Choudhury and S.L. Chaplot, Phys. Rev. B **73**, 094304 (2006).
- ³³S.L. Chaplot, N.Choudhury, S. Ghose, M.N. Rao, R. Mittal and P. Goel, European Journal of Mineralogy **14**, 291 (2002); B. Dorner, *Coherent inelastic neutron scattering in lattice dynamics*, (Springer-Verlag, Berlin)(1982); C.-K. Loong, P. Vashishta, R. K. Kalia, M. H. Degani, D. L. Price, J. D. Jorgensen, D. G. Hinks, B. Dabrowski, A. W. Mitchell, D. R. Richards, and Y. Zheng, Phys. Rev. Lett. **62**, 2628 (1989); N. Choudhury, S. Ghose, C. P. Chowdhury, C. -K. Loong, and S. L. Chaplot, Phys. Rev. B **58**, 756 (1998); K. R. Rao, S. L. Chaplot, N. Choudhury, S. Ghose, and D. L. Price, Science **236**, 64 (1987).
- ³⁴J.M. Carpenter and D.L. Price, Phys. Rev. Lett. **54**, 441 (1985); D. L. Price and K. Skold, in *Neutron Scattering*, (edited by K. Skold and D. L. Price), Academic Press, Orlando, (1986).
- ³⁵A.G. Kalinichev, J.D. Bass, B.N. Sun and D.A. Payne, J. Mater. Res. **12**, 2623 (1997).
- ³⁶The signs of the piezoelectric constants are related to the choice of the coordinate axis.
- ³⁷A. Kokalj, Comp. Mater. Sci. **28**, 155 (2003)

Table I: Calculated structural parameters and long-wavelength phonon frequencies (ω cm⁻¹) of tetragonal PbTiO₃ and rhombohedral BaTiO₃ compared with reported experimental^{1(b), 21, 22(a)} x-ray and neutron diffraction, Raman and infrared data. For tetragonal PbTiO₃, the z atomic coordinates are given in lattice units. The $R3c$ structure of BaTiO₃ is defined by the lattice constant a (Å), rhombohedral angle (in degree) and atomic displacements relative to ideal cubic positions Δ (Å). The calculated polyhedral (PbO₈, BaO₁₂) and TiO₆ octahedral distortions and bond-lengths of PbTiO₃ and BaTiO₃ are in good agreement with the experimental data. Symmetry analysis of the zone-center Γ -point phonon modes for the $P4mm$ space group of PbTiO₃ yields the classification Γ : $4A_1+5E+B_1$. The E symmetry phonon modes are doubly degenerate. For rhombohedral BaTiO₃, the phonon modes can be classified as Γ : $4A_1+5E+A_2$. The longitudinal optic (LO) and transverse optic (TO) phonon frequencies of the polar modes are listed. *The non-polar E-symmetry phonon frequency in BaTiO₃. ^aRef. [4], ^bRef. [1(b)]; ^{bb}Ref.[21(a)], ^cRef. [22(a)], ^dRef.[26(b)], ^eRef.[21(c)], ^fRef.[21(b)].

		LDA Calculations <i>This work</i>	LDA calculations ^{4, 26(a)}	Experimental ^{1(b), 21, 22(a)}
PbTiO ₃	a (Å)	3.9048	3.9048 ^a	3.9048 ^b , 3.902 ^{bb}
	c/a	1.063	1.063 ^a	1.063 ^b , 1.065 ^{bb}
	$z(Ti)$	0.5378	0.549 ^a	0.54 ^b , 0.5377 ^{bb}
	$z(O1, O2)$	0.6145	0.630 ^a	0.612 ^b , 0.6118 ^{bb}
	$z(O3)$	0.1136	0.125 ^a	0.112 ^b , 0.1117 ^{bb}
	$Pb-O$ (Å)	2.8016(4); 2.5243 (4)		2.7980 ^{bb} (4), 2.5319 ^{bb} (4)
	$Ti-O$ (Å)	1.9785 (4); 1.7606 (1); 2.3908 (1)		1.9751 ^{bb} (4), 1.7700 ^{bb} (1), 2.3860 ^{bb} (1)
	A_1 (TO) (cm ⁻¹)	146, 355, 648	151 ^a , 355 ^a , 645 ^a	147 ^c , 359 ^c , 646 ^c
	A_1 (LO) (cm ⁻¹)	187, 438, 781	187 ^a , 449 ^a , 886 ^a	189 ^c , 465 ^c , 796 ^c
	E (TO) (cm ⁻¹)	90, 170, 275, 465	81 ^a , 183 ^a , 268 ^a , 464 ^a	88 ^c , 220 ^c , 289 ^c , 505 ^c
E (LO) (cm ⁻¹)	117, 275, 416, 635	114 ^a , 267 ^a , 435 ^a , 625 ^a	128 ^c , 289 ^c , 436 ^c , 723 ^c	
B_1 (cm ⁻¹)	277	285 ^a	289 ^c	
BaTiO ₃	a (Å)	4.0	4.0 ^d	4.0 ^c
	θ (degrees)	89.90	89.85 ^d	89.90 ^c
	$\Delta_z(Ti)$ (Å)	0.053	0.043 ^d	0.052±12 ^c
	$\Delta_x(O)$ (Å)	-0.052	-0.049 ^d	-0.044±8 ^c
	$\Delta_z(O)$ (Å)	-0.080	-0.077 ^d	-0.072±8 ^c
	Ba-O (Å)	2.8286 (6), 2.7335 (3), 2.911 (3)		2.8287 ^f (6), 2.7739 ^f (3), 2.8981 ^f (3)
	Ti-O(Å)	1.864 (3), 2.147 (3)		1.8776 ^f (3), 2.1351 ^f (3)
	A_1 (TO) (cm ⁻¹)	167, 295, 527	169 ^d , 255 ^d , 511 ^d	
	A_1 (LO) (cm ⁻¹)	183, 462, 679	179 ^d , 460 ^d , 677 ^d	
	E (TO) (cm ⁻¹)	162, 240, 468, 296*	164 ^d , 206 ^d , 472 ^d , 293* ^d	
	E (LO) (cm ⁻¹)	176, 440, 688, 296*	175 ^d , 443 ^d , 687 ^d , 293* ^d	
	A_2 (cm ⁻¹)	274	278 ^d	

Table II. Calculated spontaneous polarization P (C/m²), elastic constants c_{ij} (GPa) and piezoelectric tensors e_{ij} (C/m²) of tetragonal PbTiO₃ (PT) and rhombohedral BaTiO₃ (BT) compared with reported Brillouin^{35,36} and synchrotron x-ray diffraction^{21(d)} data. ϵ^∞ and ϵ^0 represent electronic and zero frequency dielectric tensors (in units of ϵ_0), respectively.

For BaTiO₃ the tensors are in their hexagonal coordinate system, with the z -axis along the cubic (III) direction. The spontaneous polarization for PbTiO₃ and BaTiO₃ are respectively, along the cubic [001] and [111] directions. *Ref. [21(c)].

	P	c_{11}	c_{33}	c_{44}	c_{66}	c_{12}	c_{13}	c_{14}	c_{65}	e_{21}	e_{31}	e_{33}	e_{15}	e_{16}	ϵ_{xx}^∞	ϵ_{zz}^∞	ϵ_{xx}^0	ϵ_{zz}^0	
PT	Expt. ³⁵	0.75*	237	60	69	104	90	70			2.1	5.0	4.4				102	34	
	Calc.	0.78	235	45	47	99	95	69	0	0	0	2.1	4.4	6.6	0	7.6	6.9	143	26
	Calc. ¹¹		230	47	47	99	96	65				2.1	4.4	6.6					
BT	Calc.	0.28	251	236	37	89	73	36	45	45	2.3	2.3	3.7	4.6	2.3	6.1	5.5	51	27
	Calc. ^{26(b)}		277	264	48	99	79	41	45	45	2.9	3.0	4.4	5.5	2.9	6.2	5.8	69	37

Fig. 1. (Color online). (a) Computed phonon dispersion relations (full line) of tetragonal PbTiO_3 (a), rhombohedral BaTiO_3 (b) and cubic SrTiO_3 (c) compared with reported experimental inelastic neutron scattering (INS) single crystal data²⁰, optical long wavelength data^{22(a)} and reported first principles calculations⁴.

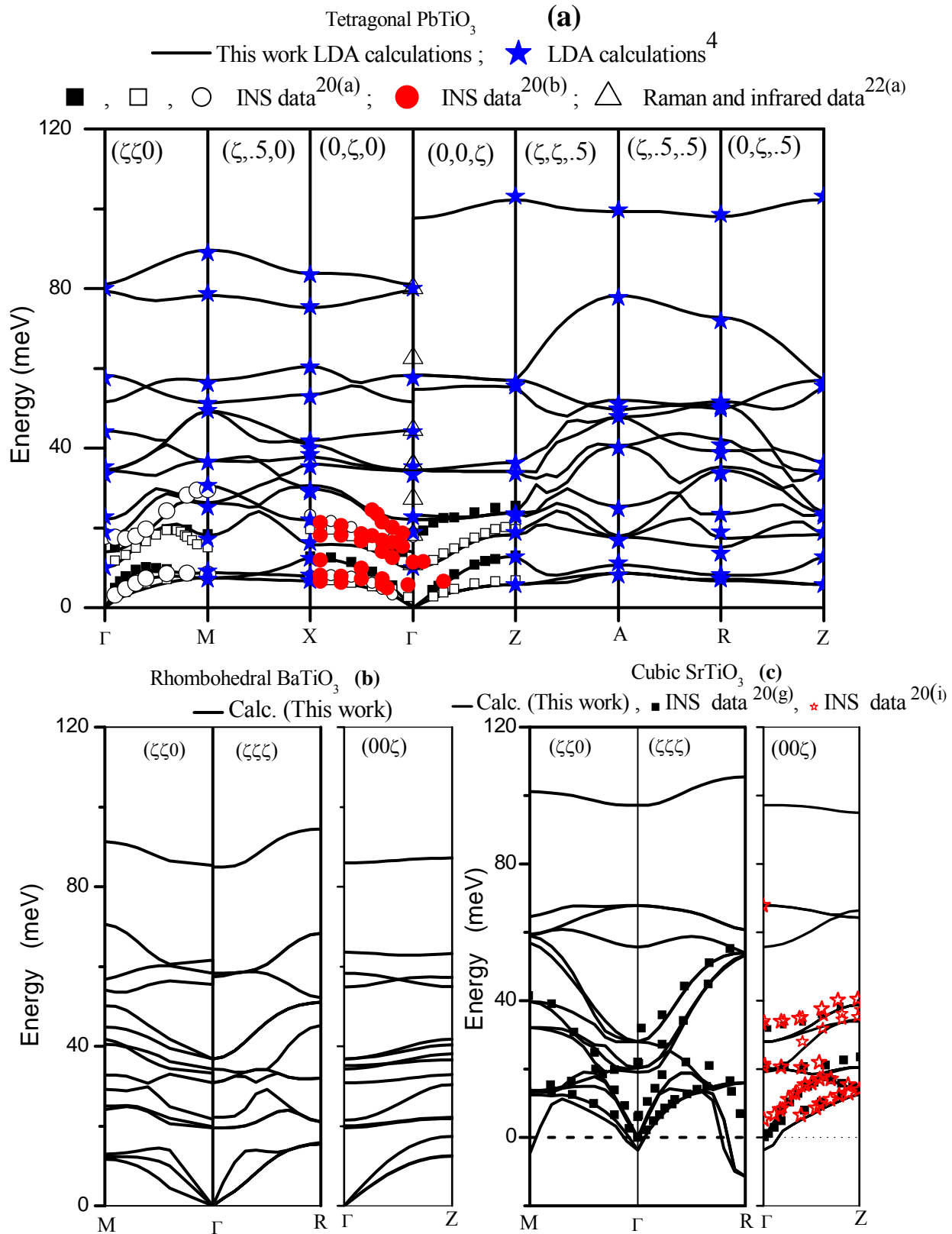
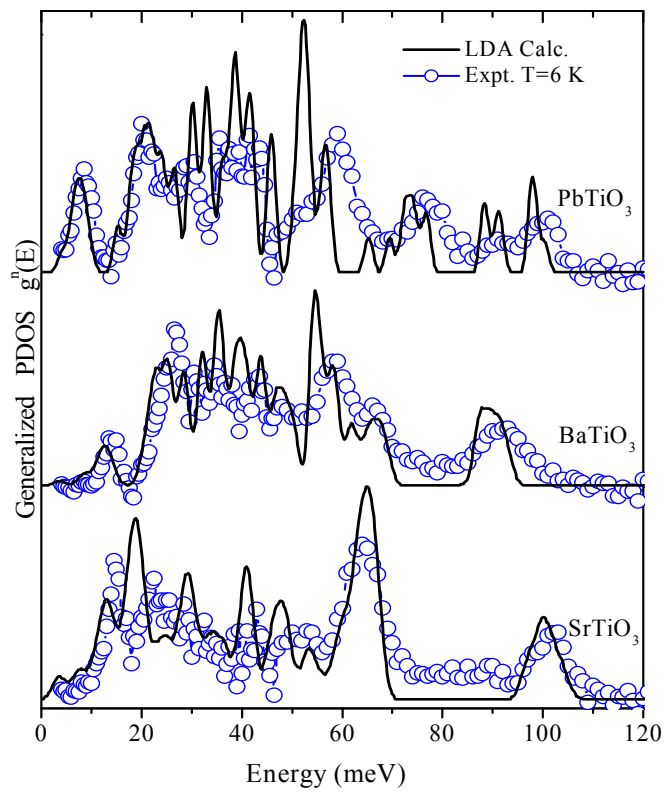


Fig. 2 (Color online). Comparison of the computed generalized phonon density of states with the measured inelastic neutron spectra ($T=6$ K) of tetragonal PbTiO_3 , rhombohedral BaTiO_3 and the quantum paraelectric SrTiO_3 .



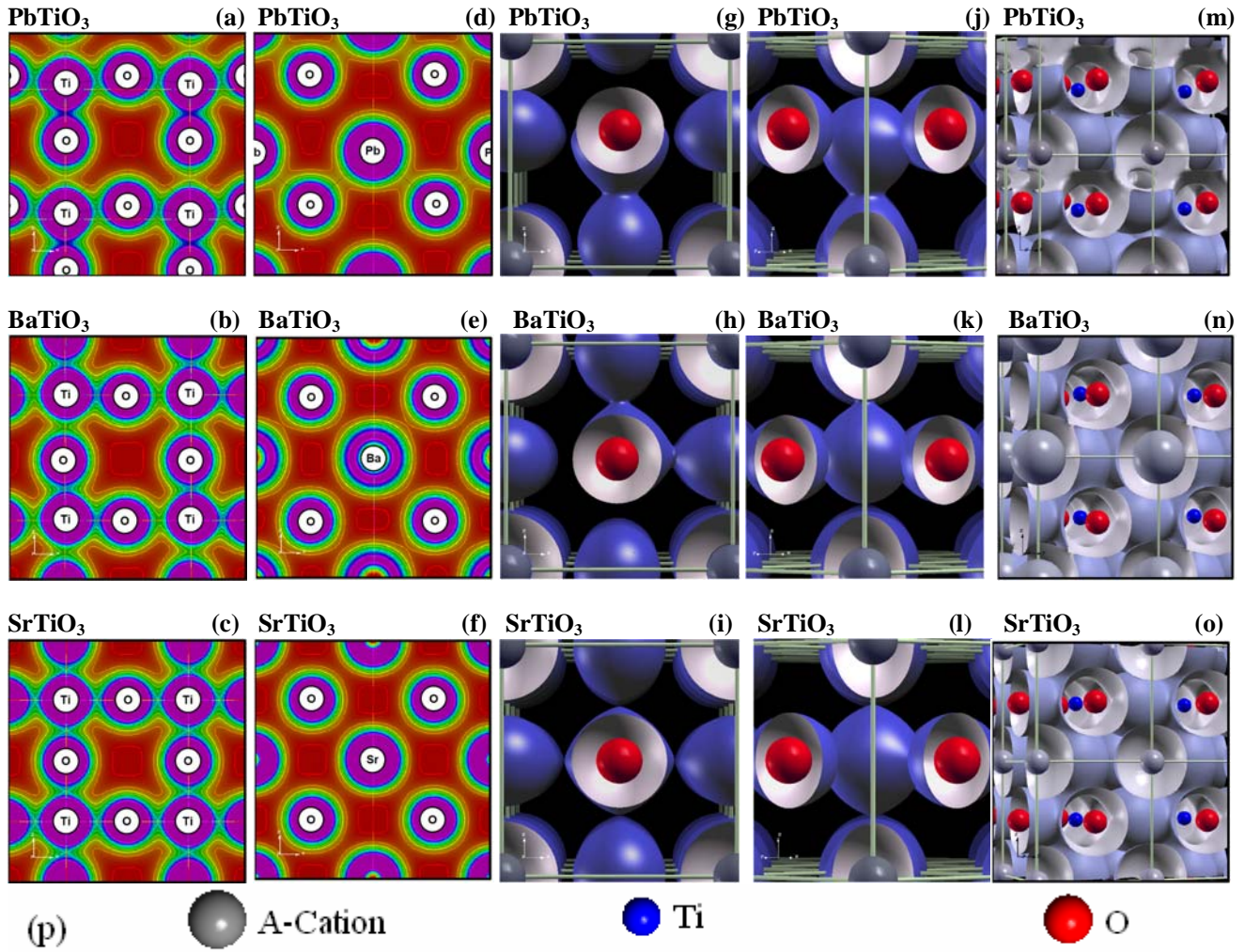


Fig. 3 (Color online). The computed charge densities (a-f) and isosurface plots (g-o) of tetragonal PT, rhombohedral BT and cubic ST displayed using the code *xcrysdn*³⁷. All densities were computed from the fully relaxed zero pressure LDA structures. The charge densities in the [010] Ti-O plane (a-c) and the [010] Pb-O plane (d-f) are shown. The 0.12 a.u. isosurfaces viewed down [100] and [110] are shown in (g-i) and (j-l), respectively, while the 0.03 a.u. isosurfaces are shown in (m-o). (p) The symbols used in (g-o) above.

Fig. 4. The computed total and partial density of states of tetragonal PbTiO_3 , rhombohedral BaTiO_3 and cubic SrTiO_3 . For cubic SrTiO_3 , effects from phonon instabilities are neglected.

